Electrodeposition of Nb_3Sn superconducting thin films

Fermilab 2019 - Summer student: M. Pozzi; Supervisor: E. Barzi

October 11, 2019

Abstract

This work is the continuation of a project born from the collaboration of Fermilab with Politecnico di Milano and further developed in last years at Fermilab. The ultimate goal of this project is to cover the internal surface of SRF cavities with Nb_3Sn which has much higher superconductive properties with respect to Nb, the material commonly used for this application. Nb_3Sn superconducting thin films are formed on Nb tapes trough the electrodeposition of Cu and Sn followed by a thermal treatment. Electrochemical parameters have been optimized to obtain a thick and continuous superconductive film. The effect of Nb surface roughness and Nb surface polishing on the adhesion of the deposited film was exploited. After the individuation of suitable electrochemical conditions for the deposition of Cu and Sn on Nb, the upscaling on cylinders was experimented. In the end, the deposition on Cu disks covered by sputtered Nb was exploited. Superconducting measurements and EDS analysis confirm the presence of a Nb_3Sn film on tapes, while cylinders and disks have not been tested so far.

1 Introduction

Nb_3Sn is an high performing type II superconducting material characterized by a critical temperature (T_c) of $18,3K$ [1] and upper critical magnetic filed of $30T$ [2]. Superconductivity in Nb_3Sn was discovered by Matthias *et al.* in 1954 [3], one year after the discovery of V_3Si, the first superconductor with the A15 structure, by Hardy and Hulm in 1953 [4].

The intermetallic niobium–tin is based on the superconductor Nb, which exists in two structures: a bcc Nb structure with $T_c = 9.2K$ or a metastable Nb_3Nb A15 structure ($Tc = 5.2K$) [5].When alloyed with Sn and in thermodynamic equilibrium, it can form either $Nb_{1-\beta}Sn_\beta$ (about $0.18 < \beta < 0.25$) or the line compounds Nb_6Sn_5 and $NbSn_2$, according to the binary phase diagram by Charlesworth *et al* [6] reported in figure 1. The solid solution of Sn in Nb at low concentrations ($\beta < 0.05$) gradually reduces the critical temperature of bcc Nb from about $9.2K$ to about $4K$ at $\beta = 0.05$ [7]. Both the line compounds at $\beta = 0.45$ and 0.67 are superconducting, with $Tc < 2.8K$ for Nb_6Sn_5 and $Tc < 2.68K$ for $NbSn_2$ [8], [9], [10], and thus are of negligible interest for practical applications because superfluid He is needed to cool down the system to such a low temperature. The $Nb-Sn$ phase of interest occurs from $\beta = 0.18$ to $\beta = 0.25$. It can be formed either above $930°C$ in the presence of a $Sn - Nb$ melt, or below this temperature by solid-state reactions between Nb and Nb_6Sn_5 or $NbSn_2$. The critical temperature for this phase depends on composition and ranges from approximately 6 to $18K$ [11].

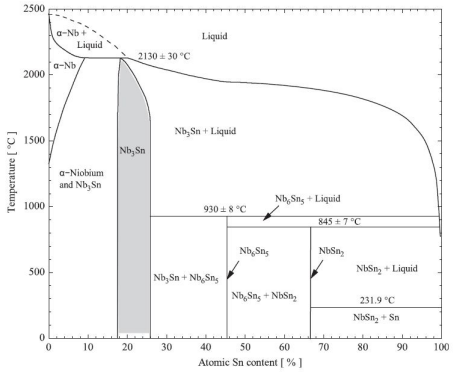

Figure 1: Nb_3Sn phase diagram [12]

So far main applications of Nb_3Sn are superconductive wires and high field laboratory magnets. Nb_3Sn wires are nowadays produced on large scale

by different techniques and are in the same time a widely studied research subject. Nb_3Sn is brittle, so wires (and mostly also magnets) are fabricated while the Nb and Sn are still separated and ductile in the wire cross-section. Usually a Cu drilled billet is used and Nb and Sn wires are inserted in the holes:the participation of Cu in the Nb–Sn reaction facilitate in some way the formation of Nb_3Sn at relatively low temperatures [13]. In general the Nb_3Sn is then formed after coil winding through a solid-state diffusion reaction at around $650°C$ in an inert atmosphere. During this heat treatment, the Sn diffuses into the Nb and reacts to form the brittle Nb_3Sn phase [2].
A further application for Nb_3Sn is to be used as internal coating for superconducting radio frequency (SRF) cavities.These are devices commonly used in particles accelerators nowadays produced in Nb:the present state-of-the-art for Nb is believed, however, to be close to the fundamental limit of the material and that is why researchers are examining the potential of alternatives to Nb with superior SRF properties [14]. Nb_3Sn seems to be a good candidate for this purpose due to its good superconducting properties, however it can't be used as a bulk material for cavity production due to its low thermal conductivity and brittle nature. Nevertheless, a thin film approach, in which a thin superconducting film is synthesized inside a cavity made out of an appropriate material, offers a promising route for exploiting Nb_3Sn for SRF use [15].
The first possibility concerning a thin film approach is to cover the internal surface of a Nb SRF cavity with a Nb_3Sn thin layer; the second one consist in the deposition of Nb_3Sn directly on a substrate other than Nb, as Cu, this allowing for the reduction of production costs for the cavity and the employment of a material with better thermal properties with respect to Nb.
Nb_3Sn can be deposited in different ways: Vapour Diffusion [16], [17], [14] and Sputtering techniques [18], [19], [20] are the most widely used, however production costs are high, deposition rates are low and the difficulty of depositing in an homogeneous way on large surfaces with curved or irregular geometries is an issue to be faced. A good alternative to these methods is electrodeposition [21], [22] a technology characterized by low production costs, high deposition rates and good scaleability of the process. In this work Nb_3Sn thin films are obtained by the electrodeposition of Cu and Sn con a Nb substrate followed by a thermal treatment during which the superconducting phase is formed.

2 Experimental setup and methods

2.1 Electrodeposition procedure

The goal of this step is to obtain a sample made of a niobium substrate covered by tree different layers obtained by electrodeposition. The first layer is a thin copper seed layer, the second one is a tin layer and the third one is a copper barrier layer. During the electrodeposition the metal to be plated is connected as cathode to the power supplier, while the other electrodes are connected as anodes. When the current is applied, positively charged ions flow from the anode to the cathode and are reduced on it and deposited as a metallic layer.
Each step is performed in a different electrochemical bath with proper electrochemical parameters, set according to the desired final thickness. According to [21] the best thickness are $1\mu m$ for Cu seed layer and $15\mu m$ for Sn and Cu barrier layer. However in different works the thickness of Cu seed layer ranges from $0.5\mu m$ to $4\mu m$, the one of Sn layer from $10\mu m$ to $60\mu m$ and the one of the barrier layer from $5\mu m$ to $15\mu m$ [23], [24].
Electrodepositions are performed in the *Legor SixStation* plating system and current is provided by *Dynatronix CRS 20-100* power supply.

Electrodes geometry

The geometry chosen for the deposition on Nb

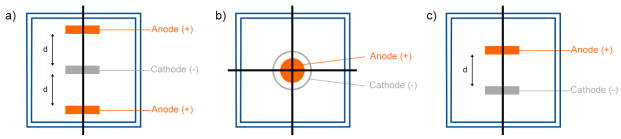

Figure 2: a) Three electrodes geometry used for the deposition of Nb plates; b) Electrodes geometry for the deposition of cylinders; c) Two electrodes geometry for the deposition of Nb/Cu disks.

plates is the one reported by Ciaccia *et al.* [23]

in which tree electrodes are used: one cathode and two anodes. The cathode (-) is placed in the center of the cell, while the two anodes (+) are placed parallel to the cathode at a distance of $2cm$ as reported in figure 2. The size of the cathode should be always smaller with respect to the size of the anodes in order to avoid shadow effect [23]: as a matter of fact, if the surface of the anode is too small, the formation of an oxide layer on the external part of the anode occurs due to side reactions, that preventing further deposition.
For the deposition on cylinders a two electrodes geometry was chosen where the two electrodes were concentric cylinders: the anode was placed in the center and the cathode at a variable distance between $1cm$ and $2cm$ as shown in figure 2.
At last also the deposition on Nb/Cu disks was performed: the disks were made of a thick Cu substrate covered by a Nb layer with variable thickness between $1\mu m$ and $5\mu m$ deposited by magnetron sputtering at *JLab*. For the deposition of Nb/Cu disks a two electrodes geometry was selected: the deposition area ($3cm$ x $4cm$) was isolated by *capton* tape before the immersion in the electrolyte and the electrical connection was provided by a copper wire as shown in figure 2.

Step 1: Cu seed layer onto the Nb substrate
The electrochemical bath composition is reported in table 1.

Table 1: Composition of the electrolyte for the deposition of Cu seed layer.

HCl	$67,8ml$
H_2SO_4	$217,4ml$
$CuSO_4$	$120g$
Distilled water	as needed to reach $2l$

The bath is prepared starting from $600ml$ of distilled water: HCl and salts are slowly added to the water in the same order as listed above. The solution is prepared in a baker at room temperature with magnetic stirring at $260rpm$ or more to help salts dissolution. It heats spontaneously up to about $80°C$ when H_2SO_4 is added and it turns to green when $CuSO_4$ is added. Before the deposition, the Nb substrate is grind with sand paper ($600 \div 800$ grid), rinsed in liquinox and etched in 49 % HF for 5 minutes to remove the oxides present on the surface. Oxide layer removal is fundamental because it decreases the adhesion of metal during electrodeposition and it acts as a diffusion barrier layer during thermal treatment, hindering the formation of the superconducting A15 phase. After the etching process, samples are degreased with acetone and the deposition area is isolated through the application of *capton* tape. It is important to be fast enough to avoid the formation of new oxides between the etching and the beginning of the first deposition. Prior to the deposition Cu electrodes are cleaned with sand paper (320 grid), citonox and acetone. During the deposition the cathode (-) is the Nb substrate and the anodes (+) are pure Cu plates. The temperature of the bath is $40°C$ and magnetic stirring is used to maintain the homogeneity of the bath. After the deposition the electrodes are rinsed in water.

Step 2: Sn layer onto the Cu seed layer
In this case a commercial electrochemical bath is used, whose composition is reported in table 2.

Table 2: Composition of the electrolyte for the deposition of Sn layer.

Solderon Acid HC	$430ml$
Solderon Tin HS-300 concentrate	$333ml$
Solderon MHS-W Primary	$200ml$
Distilled water	as needed to reach $2l$

The bath is prepared starting from $600ml$ of distilled water, then the other components are added in the order as listed above. Heating is not necessary and magnetic stirring is used to speed up the mixing. Prior to the deposition Sn electrodes are cleaned with sand paper (320 grid) and acetone. During the deposition the cathode (-) is the Cu/Nb sample while the anodes (+) are pure Sn plates. Bath temperature is $50°C$ during deposition and magnetic stirring is used to maintain the homogeneity of the solution. After the deposition the electrodes are rinsed in water.

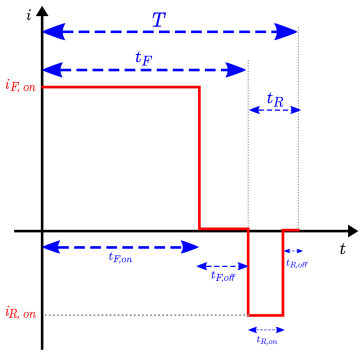

Figure 3: I vs t plot for pulsed current input [26].

Step 3: Cu seed layer onto the Sn layer
The electrochemical bath composition is reported in table 3.

Table 3: Composition of the electrolyte for the deposition of Cu barrier layer.

$Cu_2P_2O_7$	$52g$
$NaNO_3$	$10g$
$Na_4P_2O_7$	$360g$
Distilled water	as needed to reach $2l$

The bath is prepared starting from $600ml$ of distilled water, then salts are slowly added in the order as listed above. Heating at $100°C$ and magnetic stirring at are needed to improve the solubility of the salts. The solution turns to blue when $Na_4P_2O_7$ is added. Prior to the deposition Cu electrodes are cleaned with sand paper (320 grid), citonox and acetone. During the deposition the cathode (-) is the $Sn/Cu/Nb$ substrate while the anodes (+) are Cu plates. Bath temperature is $50°C$ during deposition and magnetic stirring is used to maintain the homogeneity of the solution. After the deposition the electrodes are rinsed in water.

Pulsed deposition
In order to improve the uniformity and the adhesion of the deposit, it is more convenient to use a pulsed power generator [25], [24]. As shown in figure 3, the period (T) is divided in two parts: the forward part (T_F) in which the current is positive and the reverse part(T_R) in which the current is negative. Each part is divided in two: t_{on} is the amount of time in which the current has its maximum value and t_{off} is the amount of time in which the current is zero. For our purposes T_R was set to be zero. The duty cycle (δ) can be defined as follow (1):

$$\delta = \frac{t_{on}}{T} \tag{1}$$

During t_{on} ions migrate from the anode to the cathode, while during t_{off} ions migrate away from the cathode surface: in this way fresh solution is always provided on the cathode surface, reducing the amount of nucleation sites, implying a more uniform coating. For all the depositions a period of $1000ms$ was set and a duty cycle of $0,1$ according to previous experiments by [21], [23],[24].

Theoretical deposited thickness
The amount of material deposited on the substrate can be easily computed from a theoretical point of view by Fraday's low (2) that shows the direct proportionality between the weight of the deposited material, w, and the charge provided to the cell, Q:

$$w = ZQ \tag{2}$$

The proportionality constant Z is the so called *electrochemical equivalent* which is the weight in grams produced/removed by one Coulomb in a redox reaction, and can be calculated as the ratio of one weight equivalent over the Faraday's constant (F) (3):

$$Z = \frac{w_{eq}}{F} = \frac{A_{at}}{zF} \tag{3}$$

where w_{eq} is the equivalent weight defined as the ratio between the atomic weight (A_{at}) and the number of electrons involved in the reaction.
Being V and ρ the volume and the density of the deposit, A the plated surface area, the thickness h of the deposit after a time t is given by (4):

$$h = \frac{V}{A} = \frac{w}{A\rho} = \frac{ZQ}{A\rho} = \frac{Z\sigma}{\rho} \tag{4}$$

where σ is the total charge density transferred to the sample.
Of course not all the charge provided by the power supply contributes to the reduction of the metal ions on the cathode surface, a certain amount

of the provided charge is used for side reactions as hydrogen reduction. It's possible to define a parameter, the *current efficiency*, that represents the ratio between the charge that effectively contributes to the film formation (Q_{eff}) and the total charge provided by the power supply (Q_{tot}) (5).

$$\eta = \frac{Q_{eff}}{Q_{tot}} \tag{5}$$

2.2 Thermal treatment

In figure 1 the phase diagram of the binary system $Nb-Sn$ is reported [27], [12].The single-phase Nb_3Sn is formed only above $930°C$ between 18% and 25% of Sn. At temperatures below $845°C$ the two non-superconducting phases $NbSn_2$ and Nb_6Sn_5 are also stable and they grow together with the Nb_3Sn phase. Thus, in order to minimize the formation of undesired low T_c phases, it would be necessary to reach a reaction temperature above $930°C$. Notice that if the Sn concentration is below 25% the Nb_3Sn phase remains the only thermodynamically stable phase during cool down to room temperature [28]. However, in the ternary system $Nb-Cu-Sn$, the phase Nb_3Sn is the only stable phase even at lower temperatures due to the addition of Cu. Moreover, the presence of Cu does not change too much the superconducting behavior of the material, but it decreases the formation temperature of the superconducting phase. This is the reason why before depositing Sn there should be a Cu seed layer onto the Nb substrate. The presence of Cu barrier layer instead is due to the fact that Sn melts during the thermal treatment and a barrier layer is needed to avoid Sn leaking. Thus, the $Nb/Cu/Sn/Cu$ samples undergo the heat treatment shown in figure 4 [21],[23],[24].

The first step at $206°C$ last $72h$: it is performed at a lower temperature with respect to Sn melting temperature and allows for the relaxation of internal stresses. The second step at $456°C$ last $10h$: it allows for the formation of a liquid Sn phase and during this step $Nb-Cu$ diffusion starts. After this step, an external bronze *epsilon* phase and a most internal *eta* phase are formed. The third step at $700°C$ last $24h$ and during this step the Nb_3Sn superconducting phase is formed. At the end of the thermal treatment the sample

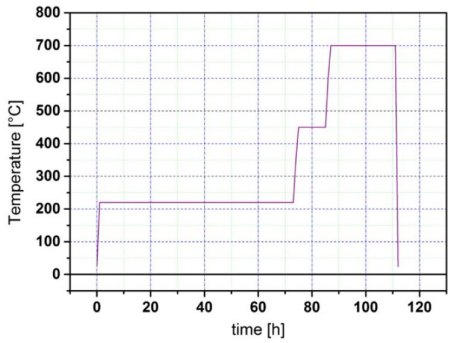

Figure 4: Thermal treatment [21]

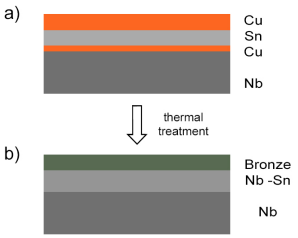

Figure 5: Schematic representation of the layers deposited on Nb substrate: before the thermal treatment(a),after the thermal treatment(b)

present a layer of$Nb-Sn$ on the substrate covered by a layer of bronze due to the diffusion of Sn in Cu barrier layer as shown in figure 5.

The heat treatment is performed using a computer controlled tubular furnace. The oven, showed in figure 6 is $1m$ long and has three different induction resistances, one at the center and two on the sides that can be separately programmed to maintain the temperature gradient as low as possible. The furnace is provided of valves for the connection to vacuum pumps and a gas tank. The samples are put on an inox sample holder, and placed at the center of the heating chamber. Before the heat treatment, vacuum is generated in the retort and argon is later inflated and let flow to avoid samples oxidation. A small internal overpressure is always maintained to avoid air reentrance. At the end of the cycle the oven is turned off, and the samples are removed when the internal temperature is lowered enough.

Figure 6: Oven for the thermal treatment, Tecnical Division, Fermilab

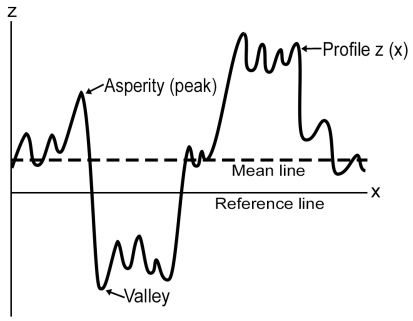

Figure 7: Example of roughness profile.

2.3 Roughness measurements

The roughness of Nb samples treated in different ways was measured with a laser confocal microscope at $10x$ magnification.
Considering a profile, $z(x)$, in which profile heights are measured from a reference line as shown in figure 7, it's possible to define a mean line (m) such that the area between the profile and the mean line above the line is equal to that below the mean line.

R_a is then defined as the arithmetic mean of the absolute values of vertical deviation from the mean line through the profile:

$$R_a = \frac{1}{L}\int_0^L |z(x) - m|\, dx \qquad (6)$$

Where:

$$m = \frac{1}{L}\int_0^L z(x)\, dx \qquad (7)$$

And R_q is the square root of the arithmetic mean of the square of the vertical deviation from a reference line:

$$R_q^2 = \frac{1}{L}\int_0^L z(x)^2\, dx \qquad (8)$$

Five extreme-value height descriptors are defined as follows: R_t is the distance between the highest asperity (peak or summit) and the lowest valley; R_p is defined as the distance between the highest asperity and the mean line; R_v is defined as the distance between the mean line and the lowest valley; R_z is defined as the distance between the averages of five highest asperities and the five lowest valleys; and R_{pm} is defined as the distance between the averages of the five highest asperities and the mean line.

2.4 SEM and EDS analysis

The cross section and the surface topography of the sample were studied using the *Scanning Electron Microscope* (SEM), whereas the composition of the coating was determined by *Electron Dispersive Spectroscopy* (EDS). These analysis were carried out both at Fermilab and at North Illinois University (NIU).
In order to look at the cross section exposing a minimum distorted surface, sample were prepared through an epoxy process. A mold was prepared by mixing $25g$ of Epoxy resin (*Epoxy wick 20-8136-128, Buehler*) and $5g$ of hardener (*Epoxy wick 20-8130-032, Buehler*). A conductive filler (*236, Buehler*) was then added to the mixture: the resin has to be conductive, otherwise there would be charge localization on the surface of the sample during the SEM analysis, producing a brighter image. The sample was hold in vertical position inside the mold by a metal clip as shown in figure 8 and figure 9. Once it got hard the mold was cut with *Buehler Isomet low speed saw.*

Then a grinding process has to be made for the front size of the mold in order to produce a smooth and flat surface. The surface of the grinder is

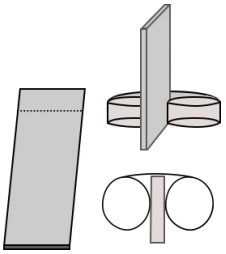

Figure 8: Sheme of he metal clip that holds the sample [24].

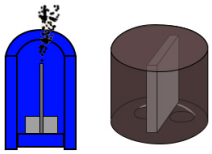

Figure 9: Epoxy process [24].

made by hard particles, whose size characterizes the level of grit of the surface. It is better to do a wet grinding with distilled water, in order to wash away the removed material of the sample, as long as the sample is not sensitive to water. With *Buheeler HandiMet roll grinder* grinding with 320, 400 and 600 grit were performed. At a fixed level of grit, the sample has be periodically dragged along the grinder surface and rotated in order to do not have a tilted surface. The angular velocity of the grinding surface was set around $100rpm$.
After that the sample undergoes a polishing process. First, it is put into a sample holder which allow to have a completely flat surface independently from tilts of the sample surface. Then the sample is moved into *Buheeler VibroMet 2*, a chamber filled with a liquid containing hard particles (SiO_2 particles in this case) and it is kept in rotation under the vibrations of the machine at a speed of 60% for a couple of days. In this machine hard particles are attached to flexible fibers which gently polish the sample surface: material removal is much slower than in grinding, that is why the process is so long. At the end of the process, the sample has to be rinsed with acetone and then dried with a blower.

2.5 Superconductivity tests

In order to perform critical current and critical temperature measurements, the sample is hold at the bottom of a probe and then inserted into a magneto-cryostat, which consists primarily of a vacuum insulated helium dewar (main bath) containing a superconducting solenoid at the bottom. In order to make measurements at different temperatures, the main cryostat feeds a second smaller helium cryostat, called *Variable Temperature Insert* (VTI), which is inserted inside the main dewar, down into the solenoid bore. Current is supplied to the sample by pressure contact between the Cu rings and two Cu lugs welded on the probe. A thin layer of indium is used to improve the electrical contact between them. All the tests were carried out on $3,8cm$ x $1cm$ samples at $4,2K$. During the test a current ramp is imposed and the resulting potential different between the electrodes is measured: by plotting $VvsI$ curve it is possible to identify when the resistance shifts from zero to a non-zero value highlighting the superconducting transition and the critical current. The test is repeated several times in the presence of different applied external magnetic field parallel and perpendicular to the surface of the sample as shown in figure 10.
In order to identify the critical current , the following criterion was used: the critical current is the value of current at which the potential difference is $0,5\mu V$. This value is computed as the product of the distance between the electrodes ($0,5cm$) and a value of the electric field of $1\mu V/cm$ that takes into account the noise of the measurement.

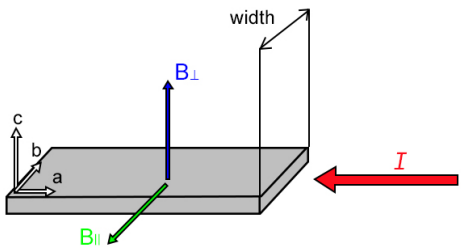

Figure 10: Scheme of sample orientation used with respect to the magnetic field B for the superconducting test [24].

3 Results and discussion

3.1 Definition of suitable current densities ranges

The first part of the work was dedicated to the individuation of the right range of current densities, for each step, that allows for the deposition of homogeneous metal layers. The starting point were the electrochemical parameters that allow for the obtainment of superconducting samples in previous experiments [23], [24].
In the first bench of experiments (samples **R42-R54**), the amount of charge provided by the power supply was kept constant among the different samples, while the current density and the duration of the deposition were changed from one sample to the other. In this way the amount of ions sent on the cathode remains the same, while the way these ions were sent continuously changed. In table 4 the electrochemical parameters for the deposition of the first bench of samples are reported.

For the first step an homogeneous and uniform Cu layer was obtained for current densities in the range $54mA/cm^2 \leq J \leq 66mA/cm^2$. At low current densities the deposition mainly occurs near the edges, where the electric field is more intense because of border effect; while at high current densities powder like deposits form on the surface as shown in figure 11.

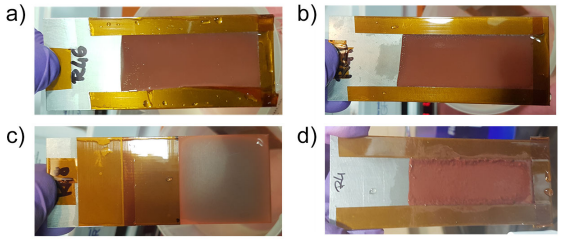

Figure 11: Pictures of some samples after the deposition of the Cu seed layer: a)Sample **R46** deposited with the right current density results homogeneous; b)Sample **R47** deposited with the right current density results homogeneous; c)Sample **R48** deposited at low current density results not homogeneous; d)Sample **R45** deposited at high current densities presents powder like deposits on its surface.

Table 4: electrochemical parameters for the deposition of samples **R42** - **R54**.

Sample Number	J (mA/cm^2)	t (min)	σ (C/cm^2)
R42	60,00	1,40	5,04
	50,00	10,40	31,20
	60,00	30,00	108,0
R43	60,00	1,40	5,04
	50,00	10,40	31,20
	60,00	30,00	108,0
R44	48,00	1,75	5,04
	40,00	13,00	31,20
	48,00	37,50	108,0
R45	72,00	1,17	5,04
	60,00	8,67	31,20
	72,00	25	108,0
R46	54,00	1,56	5,04
	45,00	11,56	31,20
	54,00	33,33	108,0
R47	66,00	1,27	5,04
	55,00	9,45	31,20
	66,00	27,27	108,0
R48	45,00	1,87	5,04
	37,50	13,87	31,20
	45,00	40,00	108,0
R49	75,00	1,12	5,04
	62,50	8,32	31,20
	75,00	24,00	108,0
R50	57,00	1,47	5,04
	47,50	10,95	31,20
	57,00	31,58	108,0
R51	63,00	1,33	5,04
	52,50	9,90	31,20
	63,00	28,57	108,0
R52	51,00	1,65	5,04
	42,50	12,24	31,20
	51,00	35,29	108,0
R53	69,00	1,22	5,04
	57,50	9,04	31,20
	69,00	26,09	108,0
R54	60,00	1,40	5,04
	50,00	10,40	31,20
	60,00	8,67	108,0

Concerning the second layer, the deposition of an homogeneous Sn layer always occur except for high current densities for which disordered powder like deposits form on the surface. The formation of such large deposit is the result of the formation of crystals already in the electrolyte that deposit on the substrate in a second time: the reduction of the cation does not occur on the surface in this case, indeed the adhesion of the film is lowered. For this step the selected range of current densities is: $J \leq 52,5 mA/cm^2$ as shown in figure 12.

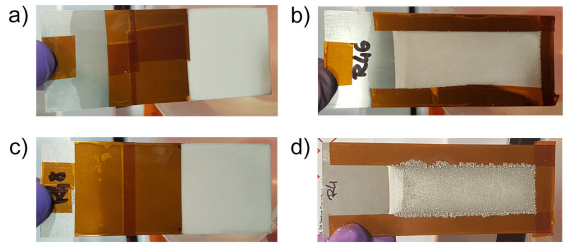

Figure 12: Pictures of some samples after the deposition of the Sn layer: a),b),c) Sample **R42**, **R46**, **R48** deposited with the right current density result homogeneous; d)Sample **R45** deposited at high current densities presents powder like deposits on its surface.

The third layer resulted to be the most complicated to be obtained: as a matter of facts for the first bench of samples, independently on the current density, the final surface results to be covered by brownish like deposits as shown in figure13.

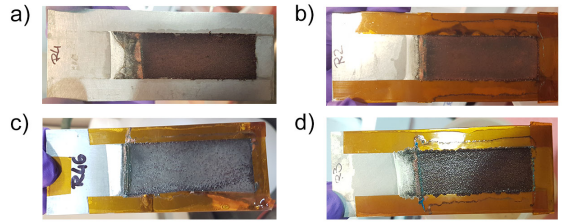

Figure 13: Pictures of some samples after the deposition of the Cu barrier layer: all the samples present oxides and powder like deposits on the surface. a)Sample **R45**; b)Sample **R42**; c)Sample **R46**; d)Sample **R43**.

This highlight the presence of Cu oxides: Cu_2O (dark red) and CuO (black). Initially it was thought that at first a thin layer of metallic Cu is deposited on Sn and then further deposition produces a layer of oxides; so by reducing the deposition time the layer of oxides was expected to be avoided. That is why samples **R42** and **R54** were deposited with the same current densities but different times. However, even reducing the deposition time, the quality of the Cu barrier layer doesn't increase. SEM images and EDS analysis of the surface of samples **R42** and **R54** are reported in figure 14.

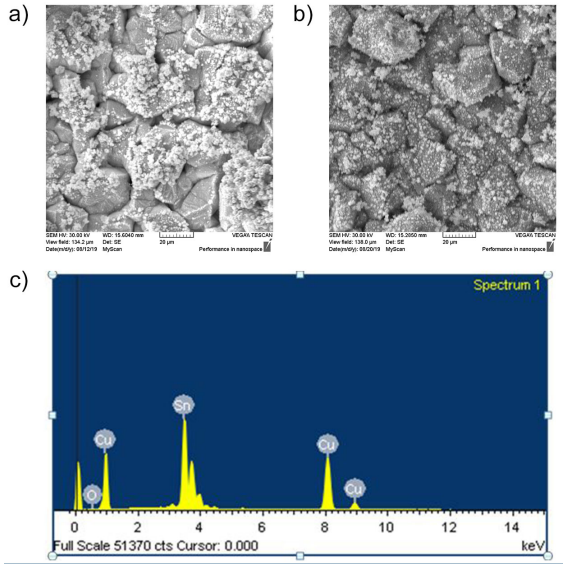

Figure 14: SEM images of samples **R42**(a), **R54**(b) and and EDS analysis of sample **R54**.

Dark grains are Sn grains while Cu is present only in the white powder deposit in form of oxides. The amount of Cu is very low and there is not the formation of a compact uniform film able to avoid Sn leakages during the thermal treatment. In figure 15 the pictures of sample **R46** after each step are shown.

Samples **R43**, **R44** and **R45** were tested but they didn't results to be superconductive, while **R46** and **R47** were superconductive. However their superconducting properties are not very good because the superconducting transition is visible only at low magnetic field and also at very low fields the critical current is not high. In figure 16 the $VvsI$ plot for samples **R46** and **R47** are re-

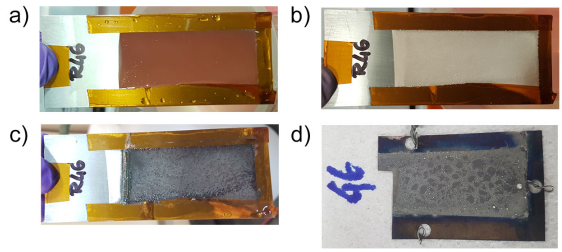

Figure 15: Sample **R46**: a)Cu seed layer; b)Sn layer; c)Cu barrier layer; d) after the thermal treatment.

ported for different value of external magnetic field.

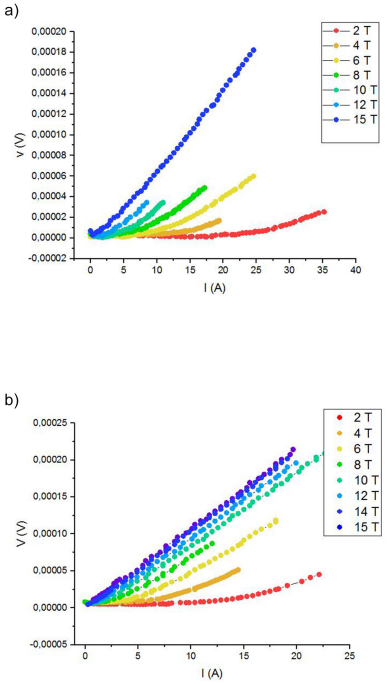

Figure 16: Superconductivity measurements of sample **R46** (a), **R47** (b).

In figure 17 SEM images of the cross section of samples **R46** and **R47** highlight the presence of a thin layer (about $4\mu m$) whose composition corresponds to Nb_3Sn covered by a layer containing Cu and Sn. In sample **R46** this layer appears quite uniform and continuous, while in sample **R47** it seems less continuous and much thinner in some regions. SEM images and EDS analysis of samples

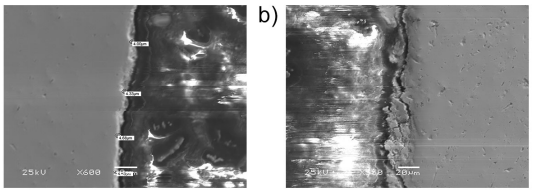

Figure 17: SEM images of samples **R46**(a), **R47**(b).

R43 and **R44** show the presence of some regions whose composition corresponds to the superconductive stoichiometric compound, nevertheless it is not possible to identify a continuous film with this composition. This suggests that in some point of the sample the superconductive phase probably has formed during the thermal treatment, but there is not a continuum film that allows for the current transportation and superconductivity measurements.

The first solution proposed to improve the quality of the third layer was to decrease the current density in order to avoid side reactions leading to the formation of oxides. A second bench of experiment was done to investigate the effect of low current densities: in table 5 the list of electrochemical parameters is reported. As starting point, samples **R55** and **R56** were deposited in the same conditions of superconducting samples obtained in previous experiments with a different electrodes geometry [24]: the quality of Cu seed layer and Sn layer resulted to be worst with respect to the samples of the first bench, while the quality of Cu barrier layer was improved. For these reasons other samples (**R57**, **R62**, **R63**, **R70**, **R71**) were deposited in the optimized conditions for Cu seed layer and Sn layer according to data acquired from the first bench of samples and with the Cu barrier layer deposited at low current densities. The deposition time was reduced in last samples to limit the formation of oxides. SEM images and EDS analysis of the surface of samples **R57** and **R63** are reported in figure 18.

These analysis show that the surface of these sample is completely covered by roundish smooth Cu grains with a small amount of oxides. The so obtained Cu layer is quite homogeneous but its thickness is still limited and not as high as desired.

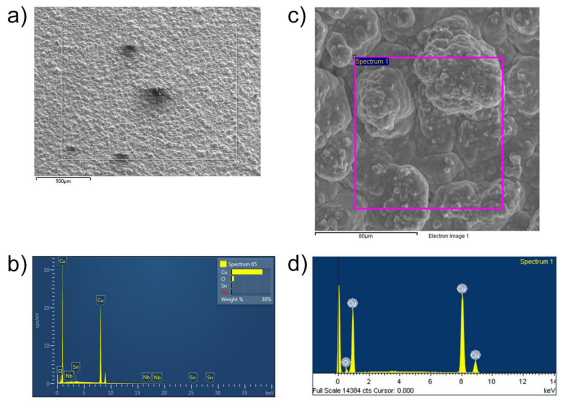

Figure 18: SEM images of samples **R57**(a), **R63**(b) and and EDS analysis of sample **R57**(c), **R63**(d).

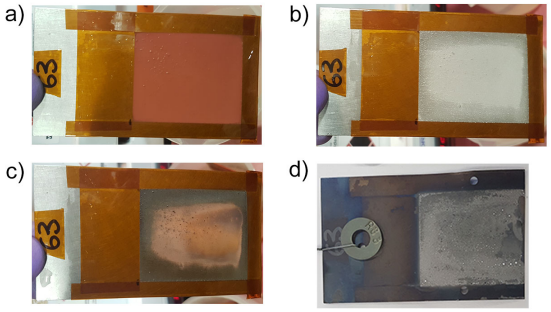

Figure 19: Sample **R63** a)Cu seed layer; b)Sn layer; c)Cu barrier layer; d) after the thermal treatment.

In figure the picture of sample **R63** after each step are shown 19.

Samples **R57** and **R63** were tested and resulted to be superconductive: in figure 20 the $VvsI$ plot is reported at different value of external magnetic field. Especially for sample **R57** the superconductive transition is visible also at higher field and at low filed the transported current is much higher than before. However these results are not as good as expected.
A second solution to the problem of the deposition of the Cu barrier layer was the deposition with direct current (DC) instead of pulsed current (PC). In this way electrons were continuously sent on the sample which was always under cathodic protection: differently from PC deposition in

Table 5: electrochemical parameters for the deposition of samples **R55** - **R57**, **R62**, **R63**, **R70**, **R71**.

Sample Number	J (mA/cm^2)	t (min)	σ (C/cm^2)
R55	17,43	2,00	2,09
	26,14	15,00	23,53
	15,25	25,00	22,88
R56	21,17	2,00	2,54
	37,06	7,00	15,57
	15,88	30,00	28,58
R57	54,00	1,56	5,04
	45,00	11,56	31,20
	15,88	30,00	28,58
R62	60,00	2,00	7,20
	45,00	12,00	32,40
	16,00	15,00	14,40
R63	66,00	2,00	7,92
	40,00	13,50	32,40
	12,00	15,00	10,80
R70	54,00	1,56	5,04
	45,00	11,56	31,20
	16,00	15,00	14,40
R71	66,00	2,00	7,92
	45,00	12,00	32,40
	16,00	15,00	14,40

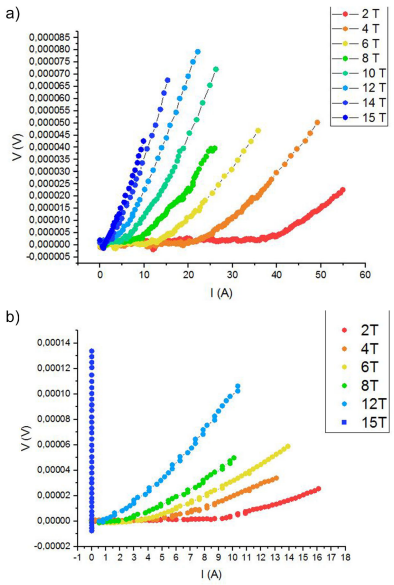

Figure 20: Superconductivity measurements of sample **R57** (a), **R63** (b).

which during t_{off} oxidation may occur, in DC deposition oxide formation should be hindered. The Cu barrier layer for samples **R59** and **R60** was deposited with DC; electrochemical parameters are reported in table 6.

For sample **R59** the deposition of the third layer was performed in basic bath in the condition reported by Reginato [25], while for **R60** it was performed in acid conditions. This choice was supported by the fact that in acid condition the deposition rate of Cu is much higher than in basic condition and the quality of the deposited

Table 6: electrochemical parameters for the deposition of samples **R59**,**R60**.

Sample Number	J (mA/cm^2)	t (min)	σ (C/cm^2)
R59	54,00	3,12	10,11
	45,00	11,56	31,21
	20,00	33,00	39,60
R60	54,00	1,56	5,05
	45,00	11,56	31,21
	30,00	17,00	30,60

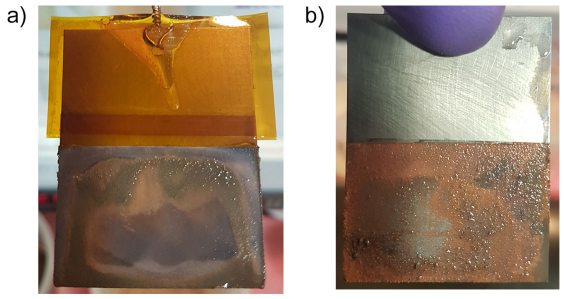

Figure 21: Samples **R59**(a), **R60**(b) after the deposition of the Cu barrier layer.

film is higher too; however in acid condition the dissolution of Sn layer may occur, that is why a basic bath was firstly selected. As expected, in basic condition a quite homogeneous Cu layer was obtained, while in acid condition the dissolution of Sn layer occurred, as shown in figure 21. SEM images and EDS analysis of the surface of sample **R59**, reported in figure 22, confirm the presence of an uniform Cu layer and a small amount of oxides. Due to the lower quality results obtained by the DC deposition with respect to low current densities deposition, this approach was non further exploited.

The last exploited solution for the deposition of Cu barrier layer was the deposition of a thin homogeneous Cu layer in basic solution that uniformly covers the Sn, followed by the deposition of a thicker Cu layer in acid solution: this technique can be defined as the *four step process*. In this way the presence of the first Cu layer hinders the dissolution of Sn once the sample is immersed in acid bath. This method was at first tested on small samples (**R67**-**R69**) to understand the feasibility of the technique and then reproduced on larger samples: in table 7 all the electrochemical parameters are reported. The final surface results to be reddish and not covered by dark oxides; SEM images and EDS analysis of sample **R76**, reported in figure 23, confirm that only Cu is present on the surface.

In figure 24 the picture of sample **R75** after each step are shown.

Sample **R73** shows a good superconducting be-

Table 7: electrochemical parameters for the deposition of samples **R61**,**R67-R69**, **R72-R76**.

Sample Number	J (mA/cm^2)	t (min)	σ (C/cm^2)
R61	60,00	0,7	2,52
	50,00	5,20	15,60
	15,88	10,00	9,53
	60,00	7,56	27,22
R67	60,00	2,00	7,20
	45,00	12,00	32,40
	16,00	5,00	4,80
	60,00	5,00	18,00
R68	66,00	2,00	7,92
	40,00	13,50	32,40
	12,00	6,67	4,80
	66,00	4,55	18,00
R69	66,00	2,00	7,92
	45,00	12,00	32,40
	60,00	2,50	9,00
	60,00	7,50	27,00
R72	66,00	2,00	7,92
	45,00	12,00	32,40
	16,00	7,50	7,20
	66,00	2,00	7,92
R73	66,00	2,50	9,90
	45,00	12,00	32,40
	12,00	7,50	5,40
	66,00	2,00	7,92
R74	66,00	4,00	15,84
	45,00	15,00	40,50
	12,00	7,50	5,40
	66,00	4,00	15,84
R75	66,00	4,00	15,84
	45,00	12,00	32,40
	16,00	5,00	4,80
	66,00	2,00	7,92
R76	66,00	4,00	15,84
	45,00	12,00	32,40
	12,00	5,00	3,60
	66,00	3,00	11,88

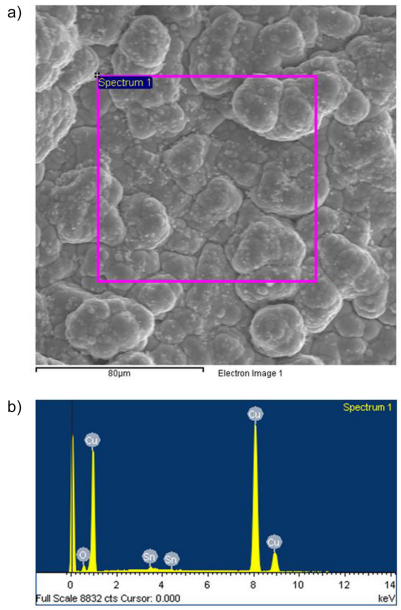

Figure 22: SEM(a) and EDS(b) analysis of sample **R59**.

havior: superconducting transition is evident also at high external magnetic fields and the critical current for low magnetic field is very high as reported in the $VvsI$ plot in figure 25. For this sample also the measurement of T_c has been done: T_c is about $17K$ but the transition is not very sharp as shown in figure 26.

3.2 Improvement of surface homogeneity

Since both electrodes are good conductors, it can be assumed that the potential difference between them is the same everywhere. As a result, the current density at any specific local area of the electrode is a function of the distance to the opposite electrode. Under this assumption, as far as the distance between the electrodes is constant (so as far as the electrodes are parallel), the current density should be the same on all the surface and the thickness of the deposit should be uniform as well. Nevertheless, on the edges of the sample, where the electric field is more intense because of border effect, the current density is more intense too. Consequently, the thickness of the deposit near the edges is higher than in the

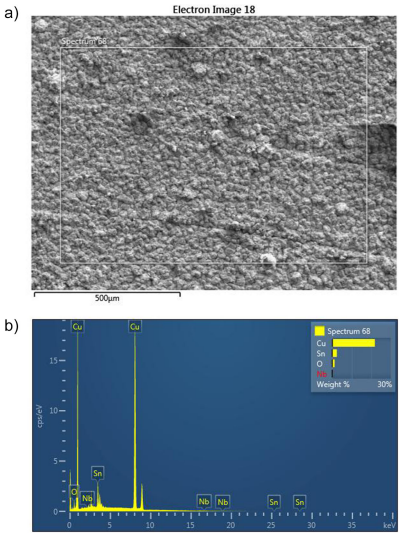

Figure 23: SEM(a) and EDS(b) analysis of sample **R76**.

center of the sample, resulting in a inhomogeneous deposition. In figure 27 there is the comparison between the theoretical and real density of flux lines and thickness.

In order to avoid this problem, an insulating tape, the *capton* tape, was used to cover the edges of the sample, reducing the border effect, allowing for a more homogeneous deposition. In figure 28 it is possible to see the comparison between the first layer deposited on a sample without the *capton* tape and one with the *capton* tape on the edges: the first one has a very thin layer deposited on the center while on the edges it is completely covered; the second one, instead, is uniformly covered.

3.3 Substrate roughness/peeling off relation

An important issue that arise from superconductive samples is that looking at a cross section with SEM, valleys with a depth of the order of some μm are present. The problem is that when trying to remove the outer bronze and level out the surface, there is the risk of creating discontinuities in the superconducting layer and to remove almost all of it [23]. In other to face this problem, Caccia *et al.* [23] deposited the tree layers on electropolished

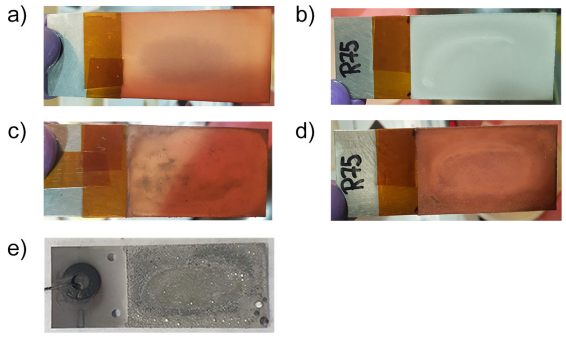

Figure 24: Sample **R75** a)Cu seed layer; b)Sn layer; c)Cu barrier layer in basic bath; d)Cu barrier layer in acid bath; e) after the thermal treatment.

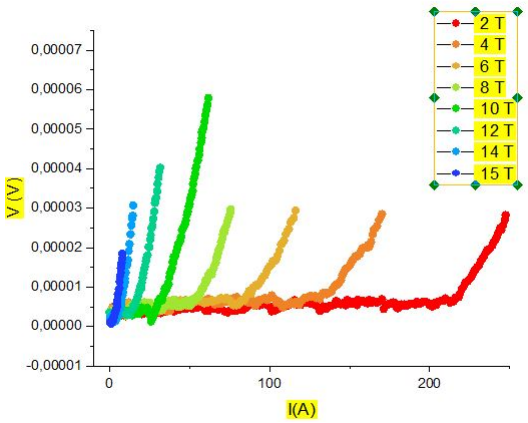

Figure 25: Superconducting measurements of sample **R73**.

samples, but delamination occurs after the end of the third step. After that they always grinded the surface of the sample before the deposition to be sure that roughness was high enough to guarantee mechanical film adhesion.

In order to determine the value of roughness necessary to obtain film adhesion and quantify in terms of roughness the difference between Nb surfaces prepared in different ways, the roughness of bare Nb, grind Nb ($600 \div 800$ grid), electropolished (EP) Nb and buffered chemical polished (BCP) Nb was measured before and after the HF treatment.

In figure 29 it is reported the image of the surface of these samples, while in table 8 the roughness values are reported. It is possible to see that

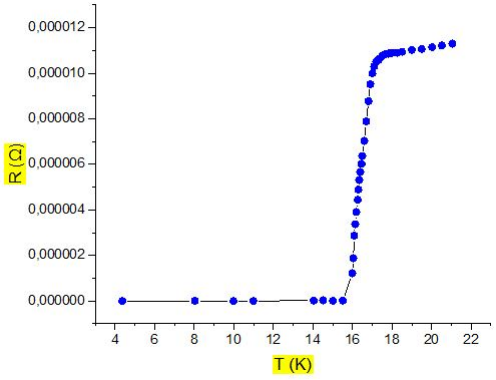

Figure 26: Tc measurement of sample **R73**.

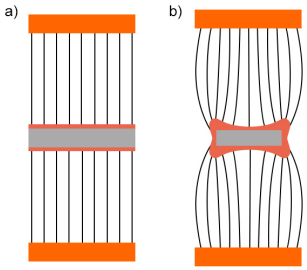

Figure 27: Schematic flux lines representation a) neglecting border effect; b) considering border effect.

bare Nb and grind Nb have the highest roughness and the value is almost the same for the two samples, meaning that the effect of grinding is almost negligible. BCP Nb has high roughness too but differently from the previous cases surface appears more ordered and rough are oriented along the polishing direction. EP Nb, in the end, has a very smooth surface and roughness is an order of magnitude lower with respect to previous cases. Moreover the effect of HF treatment (unavoidable) results only in the smoothing of peaks without affecting too much the final surface roughness value.
Samples **R64**, **R65**, **R66** were deposited in the same conditions on differently surface treated samples, not grind Nb, BCP Nb and EP Nb respectively to check for the adhesion of the film. Sample **R58** was deposited on BCP Nb too. Electrochemical parameters are reported in table 9. As shown in figure 30 on both BCP Nb and EP Nb the adhesion was so low that neither the Cu barrier layer suc-

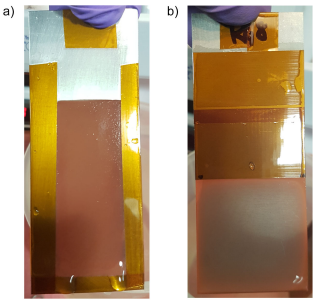

Figure 28: Cu seed layer deposited on a sample with the *capton* tape(a) and without the *capton* tape(b).

Table 8: roughness values for bare Nb, grind Nb, BCP Nb and EP Nb before and after the HF treatment.

Sample treatment	Acid treatment	Ra (μm)	Rq (μm)
bare Nb	no HF	2,149	3,314
	HF	1,788	28,10
grind Nb	no HF	2,029	2,261
	HF	1,858	3,052
BCP Nb	no HF	2,034	3,496
	HF	1,499	2,200
EP Nb	no HF	0,211	0,274
	HF	0,324	0,444

Table 9: electrochemical parameters for the deposition of samples **R58**,**R64**-**R66**.

Sample Number	J (mA/cm^2)	t (min)	σ (C/cm^2)
R58	60,00	4,20	15,12
	50,00	10,40	31,20
	15,88	30,00	28,58
R64	60,00	2,00	7,20
	45,00	12,00	32,40
	16,00	10,00	9,60
R65	60,00	2,00	7,20
	45,00	12,00	32,40
	16,00	10,00	9,60
R66	60,00	2,00	7,20
	45,00	12,00	32,40
	16,00	10,00	9,60

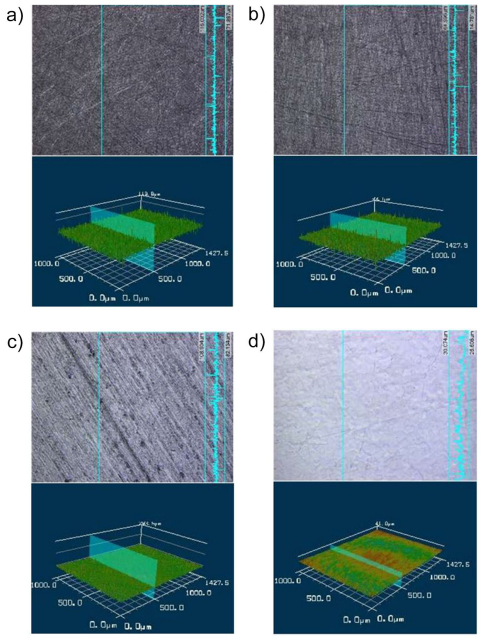

Figure 29: Surface roughness a)bare Nb; b)grind Nb; c)BCP Nb; d)EP Nb

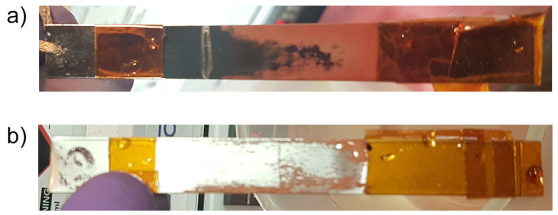

Figure 30: Poor adhesion of Cu seed layer on EP Nb(a) and BCP Nb(b).

ceed in remaining attached to the substrate: this is probably due to the fact that roughness was not high enough to guarantee good mechanical adhesion.
In the end, in the selected electrochemical conditions, not grind samples with a roughness value around $1,8\mu m$ resulted to be the more suitable substrate for the process.

3.4 Electroplating of cylinders

Once the electrochemical parameters for the deposition of rectangular tapes were defined, the upscaling to cylinders was exploited. Cylinders with $3cm$ and $5cm$ diameters were deposited with Cu seed

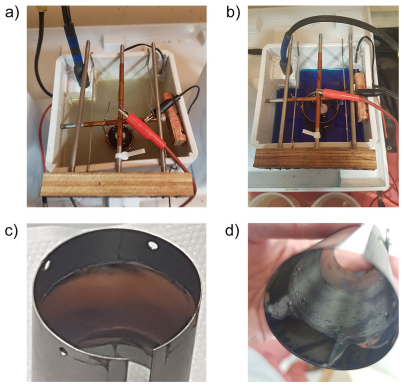

Figure 31: a)Sn deposition on small cylinder; b)Cu deposition on large cylinder; c)Sample **C5** after the deposition; d) Sample **C5** after the thermal treatment.

layer and Sn layer optimized according to previous experiments on tape, and the Cu barrier layer was deposited both at low current densities in basic conditions and with the *four step process*, half in basic and half in acid conditions. In table 10 the electrochemical parameters for the depositions of cylinders are reported.

Differently from tapes, on cylinder the *four step process* does not work very well: especially for smaller diameter cylinders, a powder like deposit is formed at the end of the fourth step and some pill off occur while rinsing the sample. A possible explanation of this problem is that smaller cylinders internal surface is only $1cm$ far from the Cu electrode, differently from tapes and larger cylinders for which the distance was set to be $2cm$. In figure 31 some pictures of the deposition on cylinders are reported: it's easy to understand the difficulty of keeping the two cylinders perfectly parallel and to avoid unwanted electrical contacts. Only sample **C6** was tested so far, but it doesn't result to be superconductive.

3.5 Deposition on Nb/Cu substrate

Once Nb was sputtered on the Cu disk at *JLab*, the thickness of Sn needed for the reaction from stoichiometric calculation was set to be the same of Nb [24]. A stoichiometric amount of Sn was chosen for sample **54**, **105** and **106** in order to avoid the formation of phases with ratio Nb/Sn

Table 10: electrochemical parameters for the deposition of samples **RC5-C13**.

Sample Number	J $(\frac{mA}{cm^2})$	t (min)	σ $(\frac{C}{cm^2})$	radius (cm)
C5	60,00	2,0	7,20	1,5
	45,00	12,00	32,40	
	16,00	10,00	9,60	
C6	66,00	2,0	7,92	1,5
	40,00	13,50	32,40	
	12,00	15,00	10,80	
C7	60,00	2,0	7,20	2,5
	45,00	12,00	32,40	
	16,00	10,00	9,60	
C8	66,00	2,0	7,92	2,5
	40,00	13,50	32,40	
	12,00	15,00	10,80	
C9	66,00	3,00	11,88	1,5
	45,00	12,00	32,40	
	12,00	7,50	5,40	
	66,00	2,00	7,92	
C10	66,00	4,00	15,84	1,5
	45,00	16,00	43,20	
	12,00	7,50	5,40	
	66,00	2,00	7,92	
C11	66,00	3,0	11,88	2,5
	45,00	12,00	32,40	
	12,00	7,50	5,40	
	66,00	2,00	7,92	
C12	66,00	4,00	15,84	1,5
	45,00	16,00	43,20	
	12,00	7,50	5,40	
	66,00	2,00	7,92	
C13	66,00	4,00	15,84	2,5
	45,00	20,00	54,00	
	12,00	7,50	5,40	

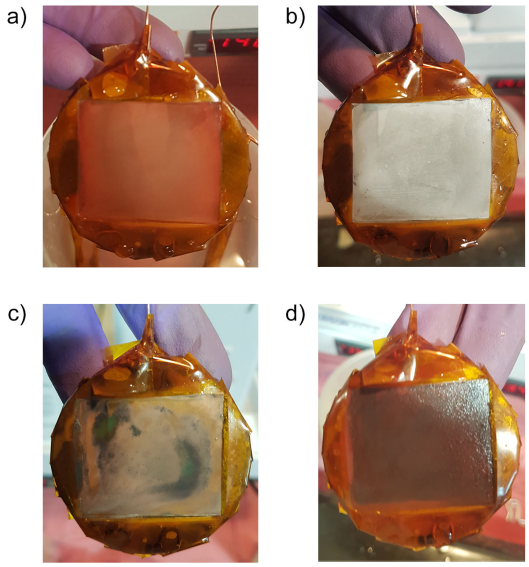

Figure 32: Sample 106: a)Cu seed layer; b)Sn layer; c)Cu barrier layer in basic bath; d)Cu barrier layer in acid bath.

lower than 3 ($NbSn_2$ and Nb_6Sn_5) during the thermal treatment. Only sample **131** was deposited with an amount of Sn higher than the stoichiometric one. Then, by knowing the right ratio between the thickness of different layers, [25] also Cu thickness was computed and trough *Faraday's low* (2) the charge to be provided by the power supply was derived taking into account an empirical value of current efficiency computed from previous experiments. All these samples were deposited with a four step process. In table 11 the electrochemical parameters derived from this computation are reported. In figure 32 the picture of sample **106** after each step are shown.

Before the deposition grinding procedure was needed in order to increase the surface roughness up to an acceptable value: the initial roughness was about $0,5\mu m$, too low to guarantee a good mechanical adhesion; the final one was about $1,3\mu m$. Even if the roughness was not as high as the one of tapes and cylinders, any detachment occurred on samples **54**, **105** and **106**. Only on sample **131**, where the amount of deposited Sn was much higher, some pill off occurred at the end of the fourth step. This is probably due to the much higher thickness of the

Table 11: electrochemical parameters for the deposition on Nb/Cu disks.

Sample Number	J $(\frac{mA}{cm^2})$	t (min)	σ $(\frac{C}{cm^2})$	Nb th. (μm)
54	$66,00$	$0,15$	$0,59$	$1,00$
	$40,00$	$0,60$	$1,44$	
	$12,00$	$7,50$	$5,40$	
	$66,00$	$0,5$	$1,98$	
105	$66,00$	$0,37$	$1,47$	$2,00$
	$40,00$	$0,80$	$1,92$	
	$12,00$	$7,50$	$5,40$	
	$66,00$	$1,00$	$3,96$	
106	$66,00$	$0,57$	$2,26$	$5,00$
	$40,00$	$2,00$	$4,80$	
	$12,00$	$7,50$	$5,40$	
	$66,00$	$1,00$	$3,96$	
131	$66,00$	$2,00$	$7,92$	$2,00$
	$40,00$	$12,00$	$28,80$	
	$12,00$	$7,50$	$5,40$	
	$66,00$	$2,00$	$7,92$	

deposited layer compared with the one of previous samples. Samples have not been baked and tested yet. What is expected for samples with a stoichiometric amount of Sn is that some Nb_3Sn would form on the surface of a thin layer of non-reacted Nb because of diffusion of Sn in Nb, while bronze would form on top because of diffusion of Sn in Cu barrier layer. In case of an higher amount of Sn, bronze would probably form both above and below the $Nb-Sn$ layer as shown in figure 33. However the diffusion of Cu trough Nb can't be avoided and it would probably affect the formation of the superconductive phase.

4 Conclusions and further perspectives

The electrochemical deposition of superconducting thin films on Nb substrate has been exploited in this work. The deposition of Cu and Sn layers on Nb allows for the obtainment of the superconducting A15 phase upon a thermal treatment during which $Nb-Sn$ diffusion occurs. As far as the quality of the deposition of the Cu barrier layer was

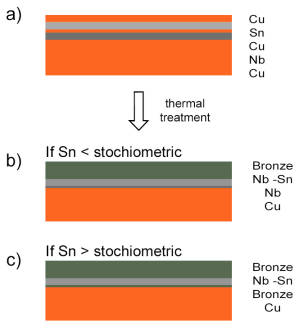

Figure 33: Schematic representation of the layers deposited on Nb/Cu disks: before the thermal treatment(a),after the thermal treatment if the amount of Sn is lower than the stoichiometric one(b) or higher(c).

improved, the superconducting properties of tested samples increased. It is important to check with the preparation of new samples the reproducibility of this technology. Moreover it would be useful for further deposition to fix the electrodes in the cell by means of plastic guides or something similar that helps in maintaining the electrodes perfectly parallel avoiding geometry related dishomogeneities.
Once the electrochemical parameters for the deposition on tapes were defined, the upscaling on cylinders was experimented: cylinders with different diameters were deposited and baked, however only the first one has been tested so far. Main issues related to deposition on cylinders are the difficulty to place the electrodes perfectly concentrical and the application of *capton* tape to isolate correctly the deposition area.
In the end the deposition on Nb/Cu disk was exploited. Samples have not been baked and tested yet. To obtain thick enough Nb_3Sn layers an higher Nb layer should be sputtered on Cu substrate. This would also simplify the electrodeposition of Cu and Sn because as deposition time increases, the control on deposited thickness is improved: it is more difficult to have a good control on deposited thickness if it is very small. At last, in order to avoid the diffusion of Cu trough Nb during the thermal treatment, a thin barrier layer (as Ta or Ti) may be sputtered between Cu and Nb.

Bibliography

[1] J. Hanak. Superconducting properties of the (nb, ta, v)3sn systems. *Phys. Rev.*, 25:342, 1964.

[2] A. Godeke, F. Hellman, H. H. J. T. Kate, and M. G. T. Mentink. Fundamental origin of the large impact of strain on superconducting nb3sn. *Superconductor Science and Technology*, 31(10), 2018.

[3] B. T. Matthias, T. H. Geballe, S. Geller, and E. Corenzwit. Superconductivity of nb3sn. *Physical Review*, 95(6):1435, 1954. Cited By :121.

[4] G. F. Hardy and J. K. Hulm. Superconducting silicides and germanides [11]. *Physical Review*, 89(4):884, 1953. Cited By :72.

[5] G. R. Stewart, L. R. Newkirk, and F. A. Valencia. Impurity stabilized a 15 nb3nb - a new superconductor. *Physical Review B*, 21(11):5055–5064, 1980. Cited By :20.

[6] I.Madsen P. Charlesworth, J.MacPhail. Experimental work on the niobium-tin constitution diagram and related studies. *Mater.Sci..*, 5:580, 1970.

[7] S. Schwartz Foner B., editor. *Superconductors Materials Science*. Plenum, New York, 1981.

[8] R. E. Enstrom. Superconducting properties of nb6sn5 and of multiphase nb-sn alloys. *Journal of Applied Physics*, 37(13):4880–4882, 1966. Cited By :3.

[9] J. P. Charlesworth. The superconducting transition temperatures of nb6sn5 and nbsn2. *Physics Letters*, 21(5):501–502, 1966. Cited By :5.

[10] D. J. Van Ooijen, J. H. N. Van Vucht, and W. F. Druyvesteyn. Superconductivity of nbsn2. *Physics Letters*, 3(3):128–129, 1962. Cited By :4.

[11] H. Devantay, J. L. Jorda, M. Decroux, J. Muller, and R. Flükiger. The physical and structural properties of superconducting a15-type nb-sn alloys. *Journal of Materials Science*, 16(8):2145–2153, 1981. Cited By :85.

[12] S. Posen and D. L. Hall. Nb3sn superconducting radiofrequency cavities: Fabrication, results, properties, and prospects. *Superconductor Science and Technology*, 30(3), 2017. Cited By :14.

[13] K. Tachikawa and Y. Tanaka. Processing of v3ga wires and their superconducting properties. *Japanese Journal of Applied Physics, Part 1: Regular Papers and Short Notes and Review Papers*, 5(9):834, 1966. Cited By :20.

[14] G. Eremeev, W. Clemens, K. Macha, H. Park, and R. Williams. Commissioning of nb3sn cavity vapor diffusion deposition system at jlab. *Proc.IPAC'15*, 2015.

[15] E. A. Ilyina, G. Rosaz, J. B. Descarrega, W. Vollenberg, A. J. G. Lunt, F. Leaux, S. Calatroni, W. Venturini-Delsolaro, and M. Taborelli. Development of sputtered nb 3 sn films on copper substrates for superconducting radiofrequency applications. *Superconductor Science and Technology*, 32(3), 2019.

[16] B. Hillenbrand, H. Martens, H. Pfister, K. Schnitzke, and G. Ziegler. Superconducting nb3sn-cavities. *IEEE Transactions on Magnetics*, 11(2):420–422, 1975. Cited By :13.

[17] M. Peiniger and H. Piel. A superconducting nb3sn coated multicell accelerating cavity. *IEEE Transactions on Nuclear Science*, 32(5):3610–3612, 1985. Cited By :8.

[18] G. Terenziani, T. Junginger, IA Santillana, S. Calatroni, and AP Ehiasarian. Nb coating developments with hipims for srf applications. 2013.

[19] Weiwei Tan, Yujia Yang, Boting Li, Li Xiao, Datao Xie, Jifei Zhao, Ziqin Yang, Deyu Yang, and Xiangyang Lu. Nb3sn thin film deposition on copper by dc magnetron sputtering. 2018.

[20] M. Durante, R. Musenich, R. Parodi, G. Gemme, P. Fabbricatore, B. Zhang, V. Boffa, V. Buscaglia, U. Gambardella, and C. Bottino. Preparation method and rf behaviour of nb3sn thin films obtained by bronze process. *IEEE Transactions on Applied Superconductivity*, 5(2):837–840, 1995.

[21] E. Barzi, M. Bestetti, F. Reginato, D. Turrioni, and S. Franz. Synthesis of superconducting nb3sn coatings on nb substrates. *Superconductor Science and Technology*, 29(1), 2015. Cited By :3.

[22] S. Franz, E. Barzi, D. Turrioni, L. Glionna, and M. Bestetti. Electrochemical synthesis of nb3sn coatings on cu substrates. *Materials Letters*, 161:613–615, 2015. Cited By :4.

[23] S.Hayato I. Ciaccia, C.Falletta. Electrochemical nb3sn film technology, 2018.

[24] S. Falletta. Optimization of superconducting nb3sn electrochemical film technology, 2017.

[25] F. Reginato. Electrochemical synthesis of nb-sn coatings for high field accelerator magnets, master thesis, 2013.

[26] G. Rosaz. Development of nb3sn coatings by multilayer sputtering for srf cavities. *Proceedings of SRF*, 2015.

[27] A. Godeke. A review of the properties of nb3sn and their variation with a15 composition, morphology and strain state. *Superconductor Science and Technology*, 19(8):R68–R80, 2006. Cited By :105.

[28] X. Xu. A review and prospects for nb3sn superconductor development. *Superconductor Science and Technology*, 30(9), 2017. Cited By :9.